Journal of Atmospheric and Solar-Terrestrial Physics 187 (2019) 22–32

Contents lists available at ScienceDirect

Journal of Atmospheric and Solar-Terrestrial Physics

journal homepage: www.elsevier.com/locate/jastp

Influence of sudden stratospheric warming on the mesosphere/lower thermosphere from the hydroxyl emission observations and numerical simulations

I.V. Medvedeva[a,*], A.I. Semenov[b], A.I. Pogoreltsev[c,d], A.V. Tatarnikov[a]

[a] Institute of Solar-Terrestrial Physics, Siberian Branch, RAS, Irkutsk, Russia
[b] Obukhov Institute of Atmospheric Physics RAS, Moscow, Russia
[c] Russian State Hydrometeorological University, Department of Meteorological Forecasts, Saint-Petersburg, Russia
[d] Saint-Petersburg State University, Department of Atmospheric Physics, Saint- Petersburg, Russia

ARTICLE INFO

Keywords:
Sudden stratospheric warming
Hydroxyl emission
Temperature
Atomic oxygen
Middle and upper atmosphere model
Atmospheric composition

ABSTRACT

We present the results of studying the behavior of temperature and of the atomic oxygen concentration in the mesopause region during the 2013 January major Sudden Stratospheric Warming (SSW). The data on the hydroxyl molecule OH(6-2), 834.0 nm emission intensity and rotational temperature were analyzed. These data were obtained through spectrometric measurements at the Geophysical Observatory of the Institute of Solar-Terrestrial Physics of the Siberian Branch of the Russian Academy of Sciences (51.8°N, 103.1°E, Tory), and at the Zvenigorod Station at the Obukhov Institute of Atmospheric Physics of the Russian Academy of Sciences (55.7°N, 36.8 E°). We calculated the concentration of atomic oxygen and its variations by using the data of the OH emission measurements. We revealed, that the response of the mesopause characteristics for two longitudinally spaced mid-latitude regions essentially differs. Thus, from the Tory Station data, the maximal increase in the OH emission intensity (by a factor of ~2) and in the concentration [O] (by a factor of ~3) occurred during the sudden stratospheric warming (SSW) evolution, whereas, from the Zvenigorod Station data, the OH emission intensity increase (by a factor of ~3) and the concentration [O] increase (by a factor of ~3.5) was observed at the SSW recovery phase. As a result of numerical modeling using the Middle and Upper Atmosphere Model (MUAM), it was shown, that the cause for the revealed effect may probably be longitudinal differences in the diurnal variation in the vertical wind at the mesopause heights over the indicated stations during the SSW. One may elucidate these differences through the generation of non-migrating tides due to a non-linear interaction between the intensified stationary planetary wave 1 (SPW1) and migrating tides and forcing a set of high-frequency PWs at the stratospheric heights. All these waves are capably of propagating into the MLT region and produce observed changes in behavior of the OH emission intensity, temperature and atomic oxygen concentration over Tory and Zvenigorod.

1. Introduction

Hydroxyl (OH) atmospheric emissions result from chemical processes at the mesopause heights and produce an ~9-km thick radiating layer with the intensity maximum at ~87 km (Baker and Stair, 1988). The hydroxyl emission spectrum represents a set of vibrational-rotational bands, mainly emitting in the IR region. The OH molecule rotational temperature determined by its emission corresponds to the atmosphere temperature at the mesopause heights (Khomich et al., 2008). The temperature and dynamic regimes in the mesopause region are characterized by a large variability caused by the influence of the solar radiation, activity of the atmospheric waves with various timescales, and many climatic and meteorological processes in the lower and middle atmosphere.

Therefore, analyzing the atmosphere characteristics at these heights may provide information on possible mechanisms for the coupling between different atmospheric layers. Winter sudden stratospheric warmings (SSWs), whose effects manifest themselves practically throughout the whole atmosphere thickness, from the troposphere (Mitchell et al., 2013) to the upper thermosphere and ionosphere (Klimenko et al., 2015; Pedatella et al., 2016), are referred to most significant meteorological disturbances encompassing large spatial and

* Corresponding author.
E-mail address: ivmed@iszf.irk.ru (I.V. Medvedeva).

https://doi.org/10.1016/j.jastp.2019.02.005
Received 14 March 2018; Received in revised form 3 September 2018; Accepted 22 February 2019
Available online 23 February 2019

time scales.

Many experimental and theoretical works concern the investigation into the SSW effect manifestation on the temperature, composition, and dynamics of the upper atmosphere. Yiğit and Medvedev (2015) showed that SSWs can cause significant disturbances in the thermosphere and ionosphere state. Tweedy et al. (2013) revealed strong variations in the MLT ozone associated with the anomalous vertical residual motion during SSWs. Pancheva et al. (2008) found dynamical coupling between the high- and low-latitude stratosphere and mesosphere during the 2003 major SSW. Medvedeva and Ratovsky (2017) revealed an increase in the OH temperature variability caused by planetary waves, tides, and internal gravity waves, during the 2016 minor SSW. Shepherd et al. (2010) reported strong atomic oxygen depletion during the 2009 major SSW and its rise during the SSW recovery phase. Wu and Nozawa (2015), by analyzing the lower thermospheric wind observations, found an enhanced semidiurnal tide before and during the 2010 SSW. Feng et al. (2017) showed a strong correlation between the temperature and the Na and Fe column densities in the Mesosphere-Lower Thermosphere (MLT) during the 2009 major SSW. Shpynev et al. (2015), collecting the data from several high- and mid-latitude ionosonde stations for the 2009 and 2013 SSWs, found that the SSW effects on the ionospheric parameters may differ for various stations depending on the ionosonde position relative to the stratospheric circulation pattern.

In this study, we present the results of the investigation of the variations in the temperature and atmosphere composition at the mesopause heights (80–90 km) for two longitudinally separated mid-latitude sites, where the Tory (51.8°N, 103.1°E) and Zvenigorod (55.7°N, 36.8°E) Observatories are located, during the 2013 January major SSW. Based on the numerical modeling using the Middle and Upper Atmosphere Model (MUAM) (Pogoreltsev et al., 2007), we attempted to explain the revealed longitudinal differences in the atmosphere temperature and composition variations observed at those stations.

2. Instrumentation and data

In this study, we use the data from spectrometric measurements of the parameters for hydroxyl emission (OH(6-2), 834.0 nm). The measurements are carried out at the Tory (51.8°N, 103.1°E) and Zvenigorod (55.7°N, 36.8°E) Observatories at nighttime, in the absence of strong cloudiness and full moon. The obtained 10-min spectra enable to determine spectral characteristics (intensity, temperature) for the hydroxyl molecule emission originating at the mesopause heights (the OH emission layer maximum is about 87 km (Baker and Stair, 1988; Khomich et al., 2008)). Measurements and data processing at both observatories are conducted through a uniform procedure. To record the spectra of the upper atmosphere airglow in the near IR region, high-aperture diffraction spectrographs equipped with highly sensitive digital CCD-cameras were used. A detailed description of the equipment and data processing technique are described in (Semenov et al., 2002; Perminov et al., 2014; Khomich et al., 2008; Medvedeva et al., 2014). The OH rotational temperature was derived by the distribution of the first three lines of the P-branch of vibrational-rotational band of OH(6-2), 834.0 nm, because, as a rule, no more than the first three lines correspond to the Boltzmann distribution of population of the rotational levels of the P-branch lines. These lines originate at quantum transitions from low rotational levels, whose populations are in the thermodynamic equilibrium, and the Boltzmann function describes their distribution. The method for determining the rotational temperature of the OH molecule was described in detail in Shefov (1961), Khomich et al. (2008). The accuracy of determining the OH rotational temperature by this technique is about 1–2 K. The hydroxyl emission intensity provides information on the concentration of reactive components at the OH emission layer heights.

To study the temperature regime and the hydroxyl emission layer maximum height variations within the investigated regions, we used satellite data from the SABER radiometer that measured the atmosphere temperature profiles and the Volume Emission Rate (VER) of OH emission. The SABER instrument is a radiometer installed aboard the TIMED satellite that measures the Earth limb emission profiles over the 1.27–17 μm spectral range. The SABER was launched in 2001 December; it operates into a circular orbit at 625 km inclined at 74° to the equator (Russell et al., 1999). To estimate the OH emission layer height, OH VER profiles of the OH (1.6 μm) were analyzed. We used the level 2A, version 2.0 SABER data obtained from the night-time passes of the satellite over the two investigated regions. For the analysis, the data within ± 7° latitude range and ± 10° longitude centered at Tory and Zvenigorod were selected.

Estimates for state of the middle atmosphere over the Northern Hemisphere during the 2013 SSW were made from the Modern ERA-Retrospective Analysis for Research and Applications (MERRA) reanalysis data, version 2. The MERRA-2 is the latest atmospheric reanalysis of the modern satellite era produced by NASA's Global Modeling and Assimilation Office (GMAO) (Gelaro et al., 2017). The MERRA-2 includes 39 time-varying product collections, all produced on a 0.625° × 0.5° horizontal grid. Variables are provided on either the native vertical grid (at 72 model layers or the 73 edges) or interpolated to 42 standard pressure levels (Gelaro et al., 2017).

Analysis of the tides and high-frequency planetary waves in the middle atmosphere was performed using new ERA5 reanalysis data (Hersbach and Dee, 2016). ERA5 data contains the hourly information on the global distribution of meteorological fields which are available at a horizontal resolution of 31 km on 139 levels.

3. Determining the atomic oxygen concentration in the mesopause region by the OH emission measurements

Hydroxyl emission results from recombination reactions of atomic oxygen produced in the atmosphere as a result of the molecular oxygen photodissociation, and is one of the channels of sink of the absorbed solar energy. The theory for producing excited OH molecules involves two basic mechanisms: ozone-hydrogen (Bates and Nicolet, 1950) and perhydroxyl (Krassovsky, 1963). Both occur in the cycle comprising two processes:

ozone-hydrogen -

$$O+O_2 + O_2 \rightarrow O_3 + O_2 \quad \alpha_{O_3}(O_2) \tag{1}$$

$$O+O_2 + N_2 \rightarrow O_3 + N_2 \quad \alpha_{O_3}(N_2) \tag{2}$$

$$H+O_3 \rightarrow OH(\, v\leq 9) + O_2 \quad \alpha_{HO_3} \tag{3}$$

and perhydroxyl -

$$H+O_2 + M \rightarrow HO_2+M \quad \alpha_{HO_2} \tag{4}$$

$$O+HO_2 \rightarrow OH(\, v\leq 6) + O_2 \quad \alpha_{OHO_2} \tag{5}$$

In this study, we use only the ozone-hydrogen mechanism, because it is responsible for, practically, about 75% of the intensity of the total emission produced by these processes.

Vibrationally excited OH molecules ($v \leq 9$) emit within the 0.5–5 μm spectral region (Semenov and Shefov, 1996) with an effective transition probability of

$$OH(\, v\leq 9) \rightarrow OH + h\nu(0.5 \leq \lambda\leq 5\mu m) \quad \bar{A} = 48\ s^{-1}, \tag{6}$$

where $\bar{A}$ is the mean effective transition probability.

The expression describing the volume emission intensity (photon·cm^{-3}·s^{-1}) at the Z height, using only the ozone-hydrogen mechanism of OH molecule emission, has the view:

$$Q_{OH}(Z) = \bar{A}\cdot\alpha_{HO_3}[H]\cdot[O_3]/\{\bar{A} + k_{O_2}\cdot[O_2] + k_{N_2}\cdot[N_2] + k_O\cdot[O]\} \tag{7}$$

where, in square brackets, the atom or molecule concentrations are designated, Z is the OH emission layer maximum height, α are the O_3

Table 1
Coefficients used in expressions (8) and (9).

1	$\alpha_{O_3}(O_2) = 5.96\ 10^{-34}\ (300/T)^{2.37}\ cm^6\ s^{-1}$	Lin and Leu (1982)
2	$\alpha_{O_3}(N_2) = 5.7\ 10^{-34}\ (300/T)^{2.62}\ cm^6\ s^{-1}$	Lin and Leu (1982)
3	$\alpha_{HO_3} = 1.4\ 10^{-10}\ (480/T)\ cm^3\ s^{-1}$	Nicolet (1989)
4	$\alpha_{HO_2} = 6.7\ 10^{-33}\ (238/T)\ cm^6\ s^{-1}$	Kaufman (1969)
5	$\alpha_{OHO_2} = 2.9\ 10^{-11}\ (200/T)\ cm^3\ s^{-1}$	Nicolet (1989)
6	$k_o = 5.00\ 10^{-11}\ cm^3\ s^{-1}$	Nicolet (1989)
7	$k_{O_2} = 1.05\ 10^{-11}\ \exp(220/T)\ cm^3\ s^{-1}$	Nicolet (1971)
8	$k_{N_2} = 3.36\ 10^{-13}\ \exp(220/T)\ cm^3\ s^{-1}$	Nicolet (1971)
9	$A = 0.91\ s^{-1}$	Langhoff et al. (1986)

molecule production coefficients, k are the coefficients for the OH molecule deactivation by atoms and molecules.

By using the obtained expression and the OH emission ozone-hydrogen mechanism, one may, based on the hydroxyl emission parameters and the known coefficients for the reaction rates, determine the atomic oxygen concentration at the hydroxyl emission layer heights (80–100 km)

$$[O] = \frac{Q_{OH}(Z)\cdot\{A + k_{O_2}\cdot[O_2] + k_{N_2}\cdot[N_2]\}}{A\cdot\{\alpha_{O_3}(O_2)\cdot[O_2] + \alpha_{O_3}(N_2)\cdot[N_2]\}\cdot[O_2]\cdot B},\ (cm^{-3}), \quad (8)$$

where

$$B = 1 - \frac{Q_{OH}(Z)\cdot k_O}{A\cdot\{\alpha_{O_3}(O_2)\cdot[O_2] + \alpha_{O_3}(N_2)\cdot[N_2]\}\cdot[O_2]}, \quad (9)$$

The coefficients used in these expressions are given in the Table 1.

By using Formula (8) and the measured values for the OH emission intensity and temperature in the OH emission layer, we calculated the atomic oxygen concentrations at the OH emission layer height for the regions, where the Tory and Zvenigorod Stations are located. We used the data from spectrometric measurements of OH emission intensity and temperature. The measured intensities were converted to the

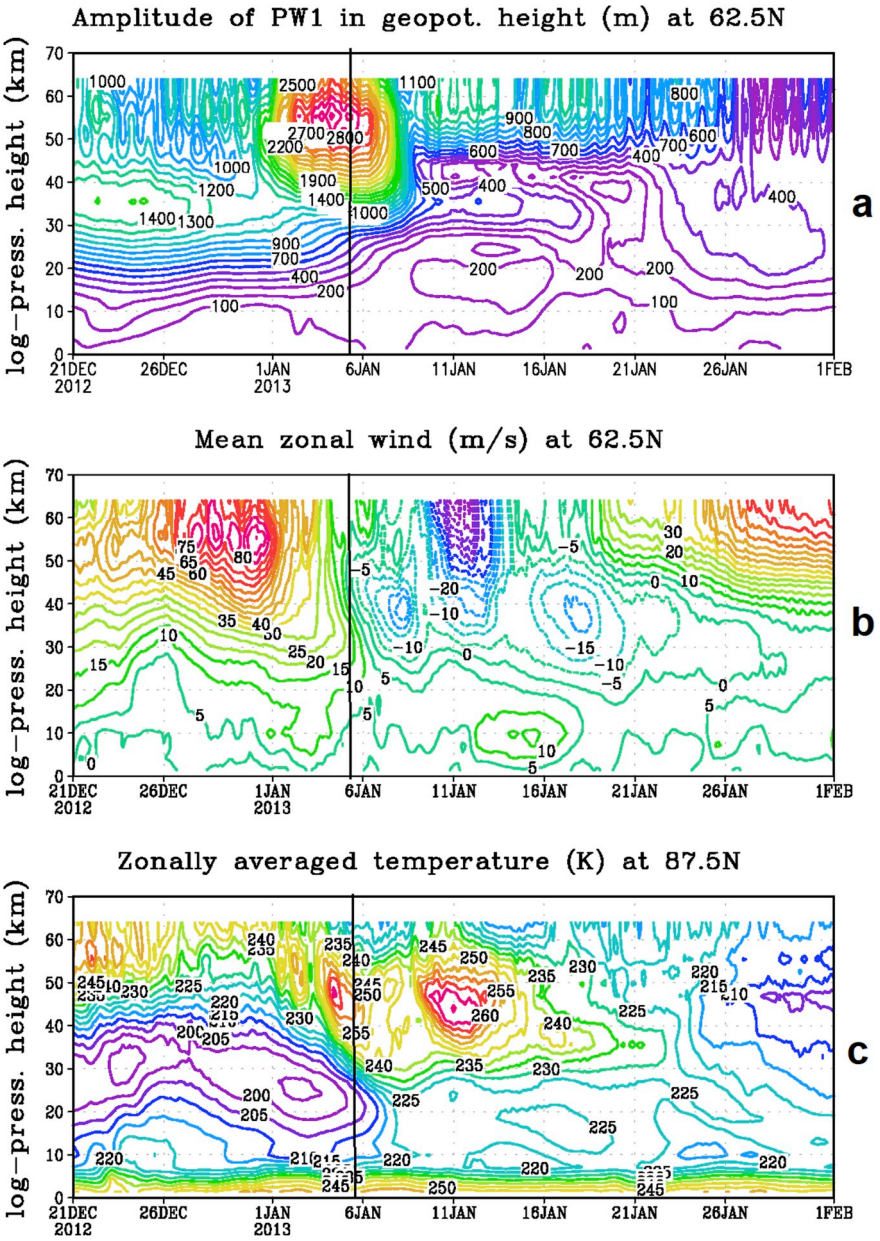

Fig. 1. Observed changes of the middle atmosphere characteristics over 2012 December 21 - 2013 February 1 (MERRA-2 reanalysis): a - amplitude of PW1 in geopotential height at 62.5 N; b – mean zonal wind at 62.5N; c - zonally averaged temperature at 87.5 N. The vertical line indicates zonal mean zonal wind reversal (62.5° N, 10 hPa).

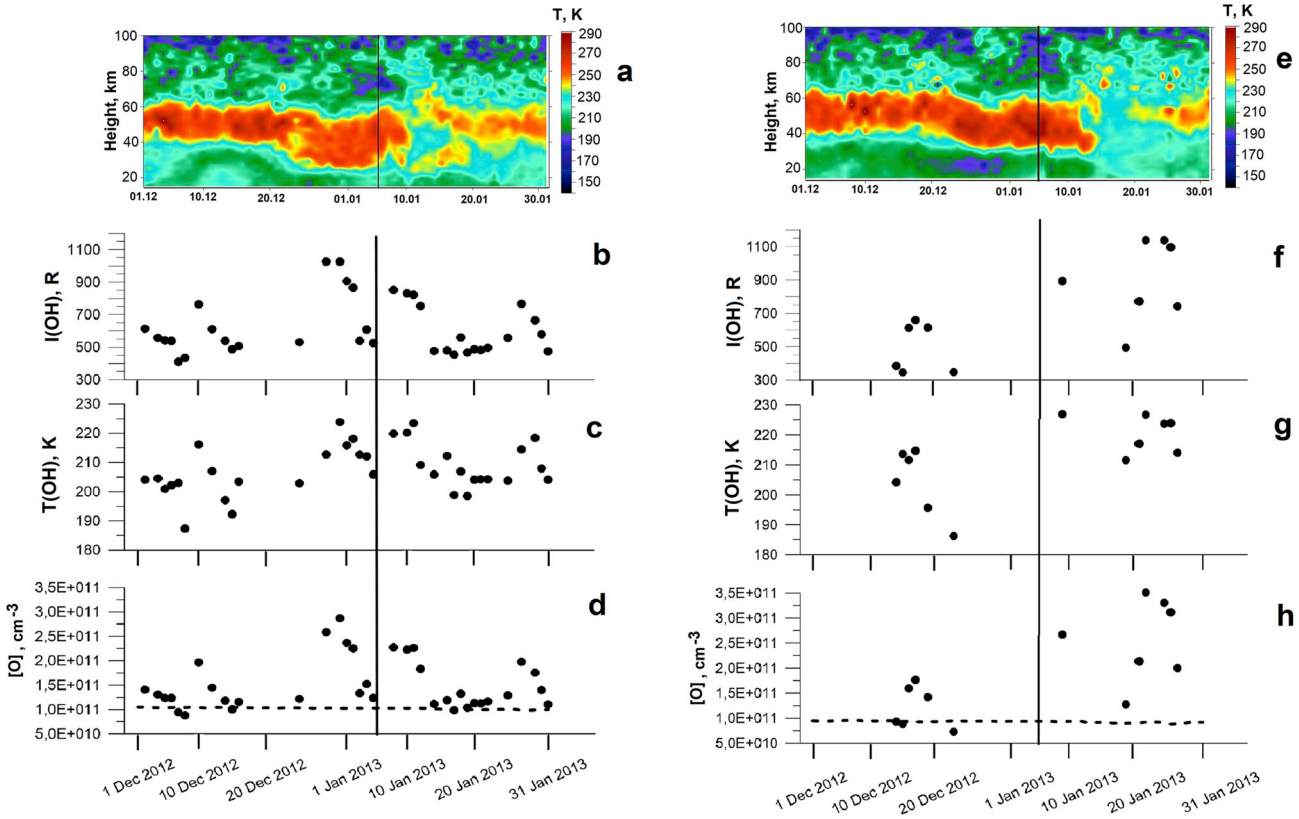

Fig. 2. Day-to-day variations in: atmospheric temperature profiles from the SABER data for the Tory (a) and Zvenigorod (e) regions; intensity of the OH emission (I (OH)) from the Tory (b) and Zvenigorod (f) ground-based data; OH rotational temperature (T(OH)) from the Tory (c) and Zvenigorod (g) ground-based data; atomic oxygen concentration [O] calculated through the above procedure for Tory (d) and Zvenigorod (h). Vertical line shows zonal mean zonal wind reversal and the major SSW onset. Dotted line is the atomic oxygen concentration from the MSIS-E-90 model.

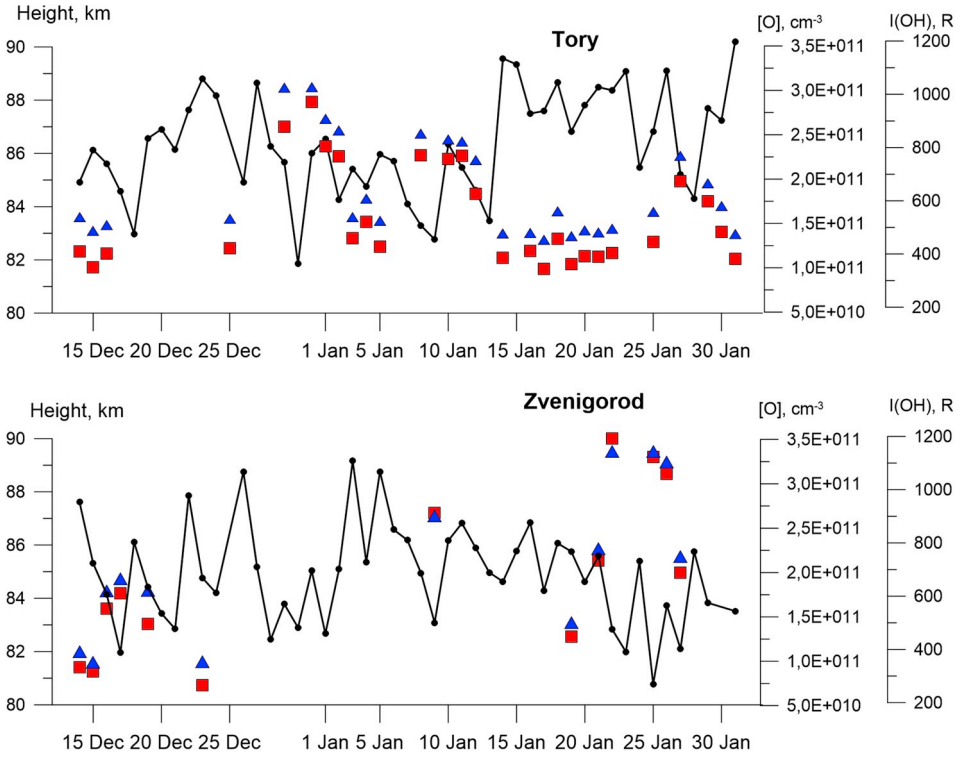

Fig. 3. Variations in the OH emission maximum from the SABER data (black), in the OH emission intensity from the ground-based data (blue triangles), and the calculated [O] (red squares). The analyzed period is 2012 December 14 - 2013 January 31.

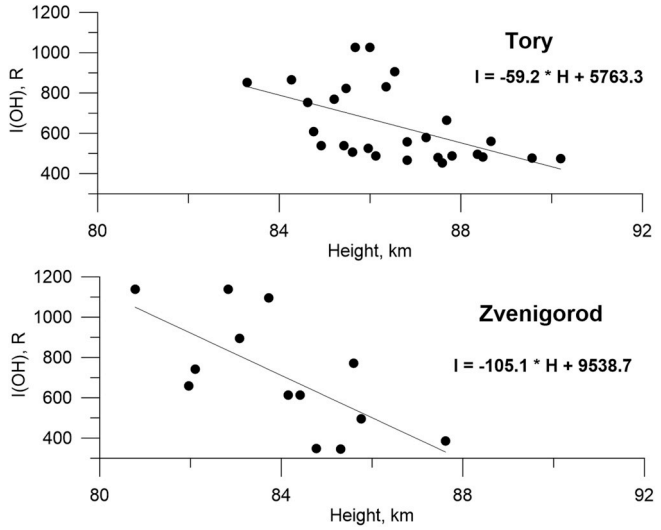

Fig. 4. Regression dependences of the OH emission intensity on the emission layer maximum height for the Tory (top panel) and Zvenigorod (bottom panel) Stations. The analyzed period is 2012 December 14 - 2013 January 31.

volume emission intensity Q in the following way. Volume emission intensity Q has dimension of photons $cm^{-3}\ s^{-1}$. The intensity obtained from ground-based measurements is in Rayleigh, i.e. its dimension is photons $cm^{-2}\ s^{-1}$. Thus, I = Q Z, and Q = I/Z, where Z is the emission layer thickness. Here, in the calculations we consider Z as equal to 10 km. The O_2 and N_2 concentrations were calculated by using the MSIS-E-90 model for each region of observation under the specified conditions: coordinates, date, time t = 0 LST. Because we do not know the exact height of the OH emission layer for ground-based measurements, we calculated [O_2] and [N_2] averaged over the 87 ± 4 km altitude range (OH layer thickness is about 9 km, OH emission layer maximum is about 87 km) (Baker and Stair, 1988; Khomich et al., 2008).

4. Results and discussion

Fig. 1 shows the behavior of the middle atmosphere characteristics during the 2012 December 21 - 2013 February 1 time interval observed in the MERRA-2 reanalysis data (Gelaro et al., 2017) [https://gmao.gsfc.nasa.gov/reanalysis/MERRA-2/] interpolated to MUAM grid points: the amplitude of planetary wave with zonal wave number 1 (PW1) at 62.5°N (a); the mean zonal wind at 62.5°N (b); the zonally averaged temperature at 87.5°N (c). The vertical line indicates reversal of the mean zonal wind (62.5° N, 10 hPa).

As the vertical coordinate, we used the log-isobaric height z = -H*ln (p/1000), where p is the pressure in hPa, H = 7 km. Up to 100 km, the log-isobaric height approximately coincides with the geopotential height. According to these data, in 2013 early January, significant disturbances of temperature and of the dynamic regime of the middle atmosphere were observed. Thus, the PW1 amplitude at 62.5°N in early January grew more than by a factor of 2 (Fig. 1a). The mean zonal wind (62.5°N, 10 hPa (~30 km)) within January 5–6 changed its direction from westerly to easterly, and persisted such until ~January 20 (Fig. 1b). The stratospheric temperature at high latitudes in late December started to increase, in early January, it increased by ~50 K and persisted increased up to January 20s (Fig. 1c). Thus, in 2013 January, a major sudden stratosphere warming evolved over the Northern Hemisphere. This SSW caused disturbances of the temperature and dynamic regimes in the middle atmosphere over a wide range of latitudes.

To study the atmosphere state in the analyzed regions of observation (Tory and Zvenigorod), we used the SABER data of the atmosphere temperature profiles obtained over 2012 December 1 - 2013 January 31. Fig. 2a presents height-temporal variations in the atmosphere temperature over the 15–100 km height range in the region of the Tory Station location from the SABER data. One can well see that, after December 22, significant disturbances of the temperature regime of the middle atmosphere were observed within the investigated region: broadening and lowering of the stratopause and the spread of the higher-temperature region from the upper stratosphere heights (~50 km) to lower heights (~25–30 km). After January 11, the structure of the middle atmosphere became nearly isothermal, without the pronounced stratopause. The stratopause formation and the recovery of a typical temperature distribution pattern started, practically, at once; however, the temperature regime of the middle atmosphere in the investigated region recovered completely only by late January, after the SSW end, when the direction of the mean zonal wind changed into westerly, and the winter pattern of the atmosphere zonal circulation over the Northern Hemisphere recovered (Fig. 1a).

The same figure presents the variations in the night-averaged values for the OH emission intensity (b) and temperature (c) obtained from the Tory Station observations, as well as the variation in the atomic oxygen concentration (d) calculated through the procedure described above. We found that, from late December, during the stratosphere warming evolution, the increase in the stratospheric temperature and in the higher-temperature region spread to the lower (to 25–30 km) stratosphere heights (Fig. 2a), one observed a substantial growth in the OH emission intensity (by over a factor of 2) and in the atomic oxygen concentration (by up to a factor of 3) as compared with the values observed prior to the SSW onset. Simultaneously, with the I (OH) and [O] growth, the T(OH) increase by ~15 K was observed. Over January 2–4, one observed a decrease in the intensity (by ~500 R), concentration (by a factor of ~2.5), and temperature (by ~15–20 K). Then, just after the moment of the mean zonal wind direction change and the major SSW onset, their values increased again. However, 5–7 days later, the values I, T, and [O] recovered to the level observed in the SSW absence with a short-time increase during the mean zonal wind direction change and the zonal circulation winter pattern recovery on January 20s. In the absence of the disturbances, the [O] calculated through the procedure stated above agrees reasonably well with the MSIS-E-90 model values (Fig. 2d, dotted line).

The right panel on Fig. 2(e–h) presents the analogous plots obtained for the Zvenigorod Station region. The analysis of the atmosphere temperature regime over Zvenigorod from the SABER data (Fig. 2e) showed the following. Like in the Tory Station region, after December 22, one observed significant disturbances of the mid atmosphere temperature regime in the investigated region. One may also note the stratopause lowering and the higher-temperature region spread to the lower stratosphere heights. However, unlike the Tory Station (Fig. 2a), the higher-temperature region spread downwards by a smaller value, without reaching 25–30 km. After January 11, the middle atmosphere structure also became nearly isothermal. But, unlike the effects observed in the Tory Station region, the stratopause formation and the recovery of the typical temperature distribution pattern in the mid atmosphere started only in late January.

Analyzing the data of ground-based spectrometric observations at the Zvenigorod Station (Fig. 2 f-h) showed that, at the mesopause heights during the SSW, the following effects were observed. Within the origin of temperature disturbances in the mid atmosphere and the SSW evolution after December 20 (Fig. 2a), a dramatic (by ~30 K) OH temperature decrease occurred (Fig. 2g). Unfortunately, because of bad weather conditions, there are no data on ground-based observations of the OH emission in the subsequent several days. However, significant changes in the MLT temperature regime from late December and a sharp decrease in the atmosphere temperature at the OH emission layer over Zvenigorod were confirmed by the SABER temperature data (Fig. 2e). At the same time, there were sufficiently low values of the OH emission intensity (Fig. 2f) and of the atomic oxygen concentration

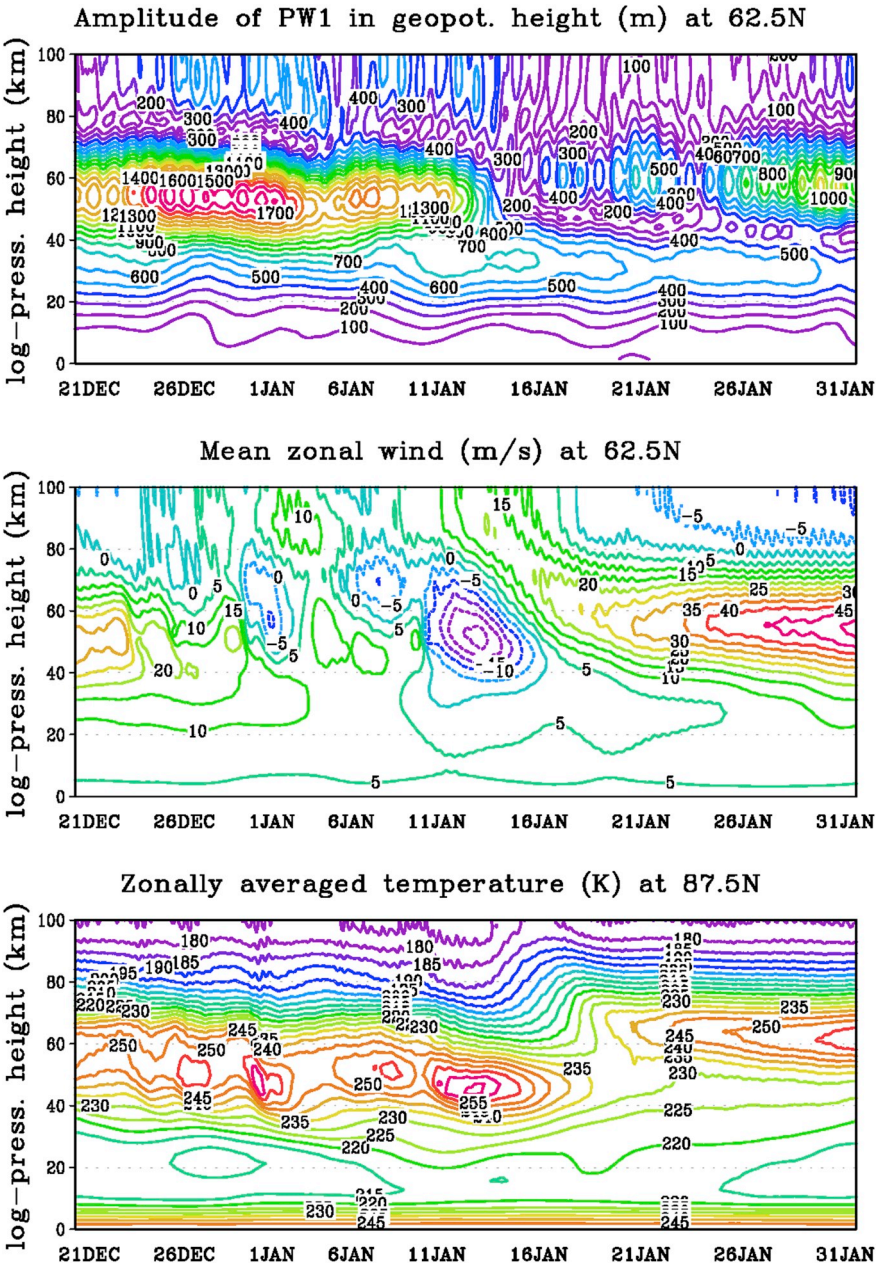

Fig. 5. Time-altitude cross-sections of the amplitude of zonal harmonic with zonal wavenumber m = 1 in the geopotential height and the mean zonal wind at latitude 62.5° N (upper and middle panels, respectively). Lower panel shows the zonally averaged temperature at latitude 87.5° N.

(Fig. 2h). During the SSW recovery phase, one observed a significant growth (by a factor of ~3) in the OH emission intensity (Fig. 2 f) and in the [O] (by a factor of ~3.5) relative to the values at the SSW onset (Fig. 2h).

Thus, the comparative analysis of the middle and upper atmosphere state during the 2013 SSW in the Tory and Zvenigorod regions revealed both common features and longitudinal differences, that is, from late December in both regions temperature disturbances within a large range of atmospheric heights were observed. After January 11, in both regions, the structure of the middle atmosphere became nearly isothermal, without the pronounced stratopause. In mid December, in both regions was observed [O] increase that continued ~7–10 days, in this time interval [O] reached up to a factor of ~2 relatively to the undisturbed conditions. One may attribute the following to longitudinal differences. In the Tory region, one observed the stratopause lowering and broadening, as well as the higher-temperature region spread to ~25–30 km. The stratopause formation and the stratosphere temperature regime recovery started practically at once. A dramatic increase in the OH emission intensity by a factor of ~2 and in the [O] concentration by a factor of ~3 occurred during the SSW evolution after December 25. Already after January 13, at the SSW recovery phase, the values of the OH emission characteristics and [O] corresponded to the conditions, when there are no disturbances, with a short-time increase during the mean zonal wind direction change and the zonal circulation winter pattern recovery on January 20s. In the Zvenigorod Station region, the stratopause started to form only in late January, after the atmosphere zonal circulation winter pattern recovery in the Northern Hemisphere. One observed the maximum of the OH emission intensity (by up to a factor of 3) and of the [O] concentration (by up to a factor of ~3.5 as compared with the values at the SSW onset) at the SSW recovery phase, like in (Shepherd et al., 2010).

In earlier studies (Yee et al., 1997; Mulligan et al., 2009; Shepherd et al., 2010) it was shown, that the OH emission intensity increased at the decrease in the OH emission layer height. We analyzed the

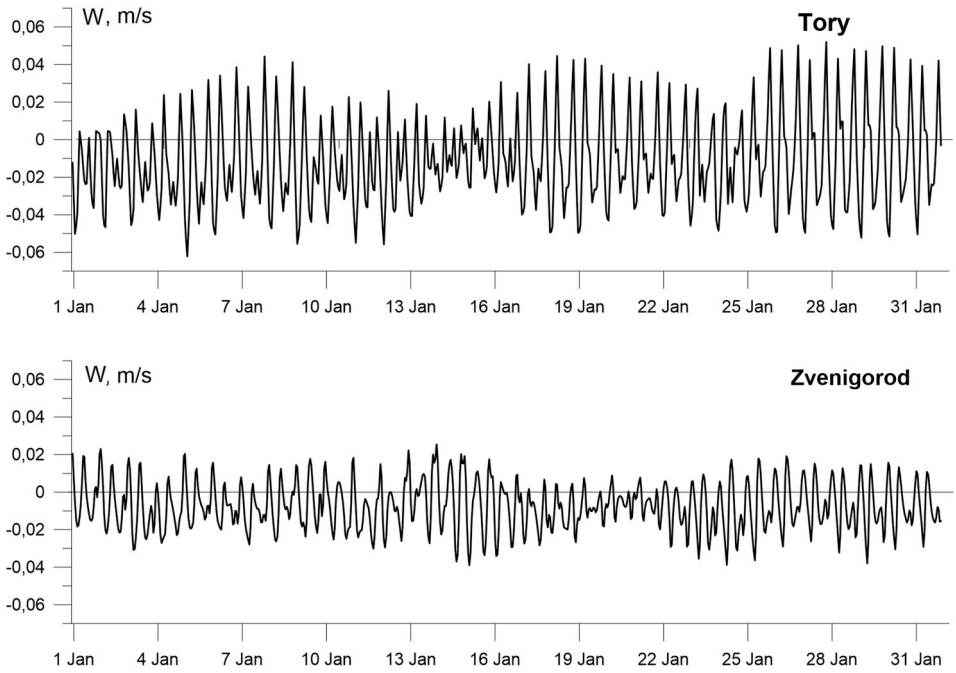

Fig. 6. Vertical wind at the hydroxyl layer height (87 km) calculated through the MUAM model for the Tory (top panel) and Zvenigorod (bottom panel) regions. Zero point on the X axis corresponds to 00 LT on January 1.

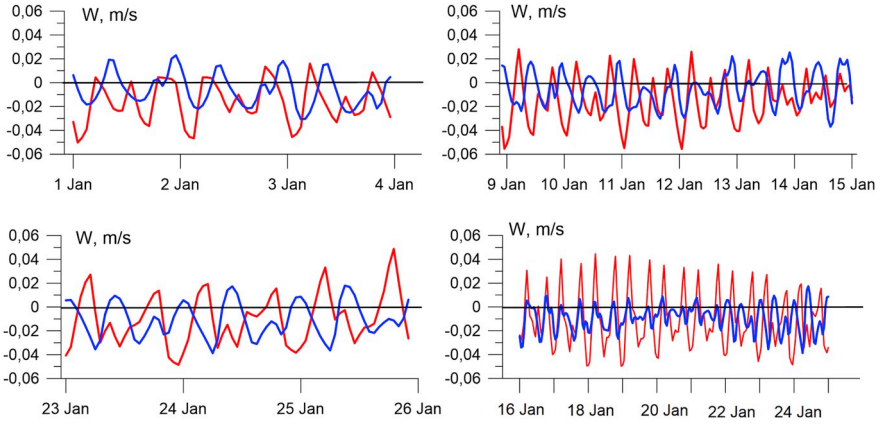

Fig. 7. Same as in Fig. 6 for separate time intervals of January for the Tory (red) and Zvenigorod (blue) regions.

variations in the OH emission layer height. For this, we involved the SABER data on the OH volume emission rate (VER) profile. For the analysis, we used of the OH 1.6 μm VER profiles, level 2A, version 2.0. In (Mulligan et al., 2009; Shepherd et al., 2010) were shown, that the OH layer maximum height at limb measurements from the satellite and from the VER OH ground-based measurements are in an inverse correlation dependence. Therefore, to estimate the variations in the hydroxyl emission layer height, we used the data on the OH emission maximum height obtained from the SABER measurements of the hydroxyl emission profiles. For each VER profile, we determined the emission maximum height. Fig. 3 presents the results. The top panel corresponds to the data for the Tory Station region, the lower panel shows the same for the Zvenigorod Station region. Black color indicates the variations in the OH emission maximum from the SABER data, dark blue triangles correspond to the OH emission intensity from ground-based data, red squares designate the calculated the [O] concentration. The analyzed period covers 2012 December 14 - 2013 January 31.

From the plots, one can see that between the hydroxyl layer maximum height and the OH emission intensity and the atomic oxygen concentration, there is an inverse dependence. Thus, for the Tory region, at the SSW evolution phase in late December - early January, a dramatic growth in the OH emission intensity and the atomic oxygen concentration were accompanied by lowering of the emission layer height to 82 km (Fig. 3, top panel). But already after January 12, the OH layer height values measured with the satellite were 87–88 km, and the I(OH) and [O] over that period returned to the values observed prior to the SSW onset (top panel).

For the Zvenigorod region, a significant lowering of the OH layer was observed after January 16, at the SSW recovery phase. On January 25, the layer height reached the minimal value of 81 km (Fig. 3 bottom panel). In this period, I(OH) and [O] reached maximal values.

Fig. 4 presents regression dependences between the OH emission intensity and the emission layer maximum height for the Tory Station (top panel) and for the Zvenigorod Station (bottom panel). For both regions of observation, one can clearly see anticorrelation between the hydroxyl emission intensity and the height. Over the analyzed period, the OH emission maximum height varied from 83 km to 90 km for the Tory region and from 81 km to 88 km for the Zvenigorod region.

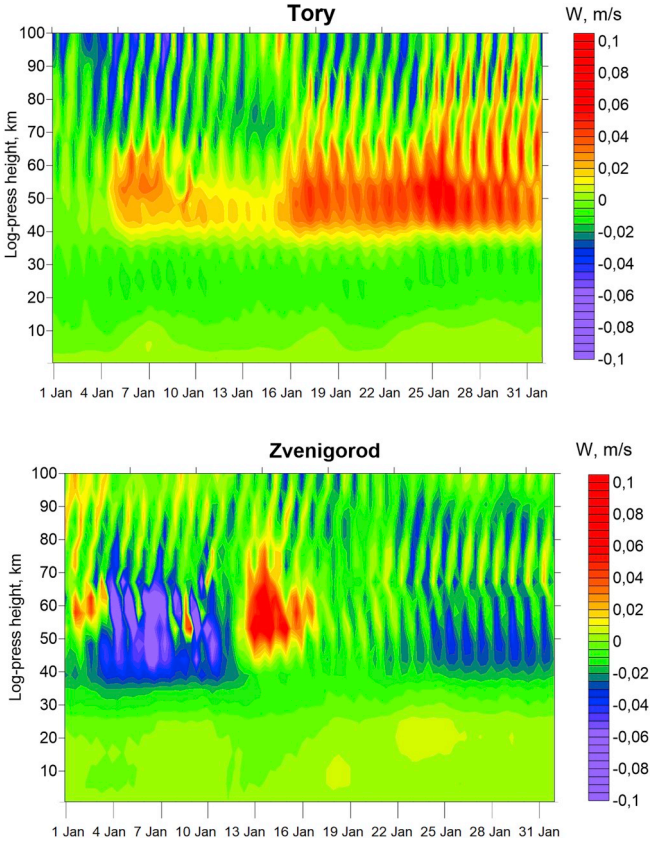

Fig. 8. Height-temporal variations in the vertical wind calculated for the Tory (top panel) and Zvenigorod (bottom panel) regions by the MUAM model.

5. Numerical simulation with the Middle and Upper Atmosphere Model

To reveal possible causes for the observed longitudinal differences of the I(OH), T(OH), and [O] variations at the Tory and Zvenigorod Stations, we performed numerical modeling for the dynamics of the vertical component of wind velocity in the atmosphere over the 0–100 km height range. To model the thermal conditions and the common atmosphere circulation, we used the Middle and Upper Atmosphere Model (MUAM) (Pogoreltsev et al., 2007). The MUAM represents a 3D non-linear model for the common atmosphere circulation. The model is implemented at a grid, 5.625° in longitude, 5° in latitude. As a vertical coordinate, the log-isobaric height z = - H*ln (p/1000) is used, where p is the pressure at hPa, H = 7 km. The height step is 0.4*H, and there is a possibility to set an arbitrary number of vertical levels from 48 to 60. In this study, we used the 56-level MUAM version. The time integration step was 225 s. In the last MUAM version, new parameterizations were involved: effects of orographic gravity waves (Gavrilov and Koval, 2013) and normal atmospheric modes (Pogoreltsev et al., 2014). The lower boundary conditions at 1000 hPa were set in the form of averaged horizontal distributions of the geopotential heights and temperature for January. Those distributions were obtained from the JRA reanalysis data (Japanese 55-year Reanalysis) (Kobayashi et al., 2015). To reproduce the conditions closest to the observed ones within the 2012–2013 winter in our numeric calculations, we (when calculating the lower boundary conditions) averaged the distributions for 1982, 1991, 1994, 2002, and 2004, during which the ENSO neutral phase according to the Multivariate ENSO Index (MEI) [http://www.esrl.noaa.gov/psd/enso/mei/table.html] was observed. Besides, ensemble calculations were conducted for the quasi-two-year variation westerly phase conditions (Pogoreltsev et al., 2014). Unfortunately, it is difficult to estimate the errors of simulated vertical wind. Nevertheless, the comparison of vertical wind obtained with the MUAM and using the radar measurements shows a good agreement (Portnyagin et al., 2010, 2011).

To include the latent heating due to condensation, the Modern-Era Retrospective Analysis for Research and Applications (MERRA) convective precipitation data were used for the selected years (Rienecker et al., 2011). The distribution of heating rates is calculated by using the empirical formula from Hong and Wang (1980):

$$J(z, \lambda, \varphi) = J_Z(z)\, J_{\lambda\varphi}(\lambda, \varphi), \tag{10}$$

where $J_{\lambda\varphi}(\lambda, \varphi)$ is the observed longitude/latitude distribution of precipitation rates near the ground and $J_z(z)$ is the empirical formula for the vertical distribution of the latent heating rates depending on the precipitation rate near the ground:

$$J_Z(z) = A \left\{ \exp\left[-\left(\frac{z - 6.5}{5.39} \right)^2 \right] - 0.23 \exp\left(-\frac{z}{1.31} \right) \right\}, \tag{11}$$

here A is the empirical constant, which was obtained based on the measurements (Reed and Recker, 1971). A = 8.54 mW/kg corresponds to the rainfall rate of 1.6 mm/day.

The procedure for numerical experiments matched the one described in (Pogoreltsev et al., 2007), i.e., until model day 330, we used the Sun fixed zenith angle corresponding to the January 1 conditions; then, its seasonal variations were involved. In summary, model days 330–400 corresponded to January–February and early March. As a result, we obtained a solution ensemble involving 10 terms by using different initial conditions. For the further analysis, selected was one of the versions, when the SSW event evolved in the first half of January (see Fig. 5). Although the model SSW (Fig. 5) is a little weaker than that observed in 2013 January (Fig. 1), the basic features of the vertical wind behavior over Zvenigorod and Tory (longitudinal differences) may be estimated, at least, qualitatively based on modeling calculations.

Fig. 6 presents the results of modeling the vertical wind at the hydroxyl layer height (87 km) for the Tory (top panel) and Zvenigorod (bottom panel) regions. The horizontal line marks the wind velocity zero value. The «+» sign corresponds to the upward wind, the «-»-downward. The calculations showed that the vertical wind velocity for the Tory Station varied over −0.06 to 0.04 m/sec, with −0.04 to 0.02 m/sec for the Zvenigorod Station.

From the figure, one can see that the prevalent vertical wind for the Tory Station over January 1–4, 9–15, and 23–26 was downward (see Fig. 6, top panel) during both nighttime and daytime. It is these periods, when we found an increase in the OH emission intensity, an increase in the atomic oxygen concentration, and a decrease in the hydroxyl emission layer height from the experimental data. The model calculations for the Zvenigorod region showed that the downward vertical wind was observed at the SSW recovery phase, on January 16–25. Fig. 7 shows the discussed time intervals zoomed in.

Fig. 8 presents the results of the vertical wind profile model calculations for the Tory (top panel) and Zvenigorod (bottom panel) regions. The zero point on the X axis corresponds to 00 LT on January 1. From the figure, one can see that, for the Tory Station, the prevalent wind within 80–90 km (hydroxyl emission layer height) is mainly downward until mid January, whereas, in the second half of January, the prevalent wind is upward. For the Zvenigorod region, after January 16, a sufficiently strong vertical downward wind at 80–90 km prevailed.

Thus, the hydroxyl emission layer significant variations causing changes in the OH emission intensity and in the OH temperature, as well as in the atomic oxygen concentration, at the mesopause heights, may result from the vertical wind variations within the atmosphere.

The downward vertical wind leads to lowering of the OH emission layer, which result in its adiabatic heating. As a result, there is an increase in the OH temperature, in the atomic oxygen concentration, and, as a consequence, an increase in the OH emission intensity. In case of

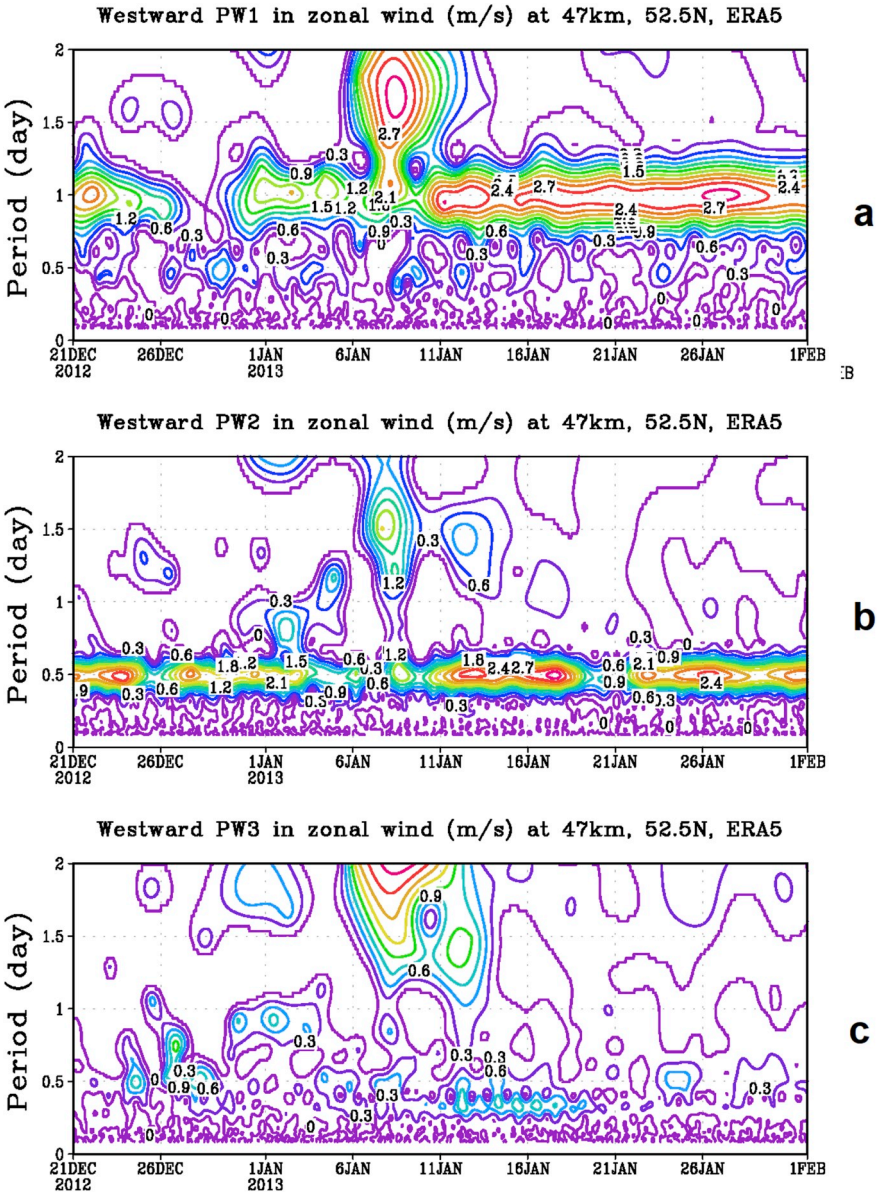

Fig. 9. Observed changes of amplitude wavelet spectra for westward propagating PWs in meridional wind (ERA5 reanalysis) at 47 km, 52.5° N: a – zonal wave number 1; b – zonal wave number 2; c - zonal wave number 3.

the vertical upward wind, on the contrary, there is an increase in the OH emission layer height, which leads to an adiabatic cooling, to a decrease in the OH temperature, in the atomic oxygen concentration, and in the OH emission intensity. Similar results and conclusions, as well as a possible mechanism elucidating the [O] change at upward/downward motion, were presented and discussed in (Shepherd et al., 2010). According to that paper, an increase in the atomic oxygen concentration at the OH emission height occurs due to an influx of atomic oxygen from the thermosphere, where its concentration is considerably higher, than that in the mesopause region. As a result of the upward motion, air masses with a low content of atomic oxygen arrive at the OH emission layer heights from the lower atmosphere (Shepherd et al., 2010). In (Shepherd et al., 2010), there are estimates for the velocity of the vertical motion leading to variations in the OH layer height during the 2009 stratospheric warming. The authors assume that, in that period, the OH emission layer height variations occurred due to a vertical motion with a rate of 1 km d^{-1}, or 0.01 m s^{-1}.

The model calculations showed the existence of longitudinal differences in the vertical wind variations over Tory and Zvenigorod regions. These differences agree well with the revealed effects from the experimental ground-based and satellite data. The obtained differences in the vertical velocity diurnal variations over the indicated stations during SSW events may be elucidated by generation of non-migrating tides as a result of non-linear interaction between the increased SPW1 and migrating tides (Pogoreltsev et al., 2007). To check such possibility, the wavelet analysis of the tides and high-frequency planetary waves in the stratosphere has been performed using new ERA5 reanalysis data (Hersbach and Dee, 2016). ERA5 data provide us with the hourly information on the global distribution of meteorological fields and we have a possibility to investigate the characteristics of the main tidal oscillations. A complex wavelet analysis using Morlet mother wavelet (Torrence and Compo, 1998) has been applied to the time series of the real and imaginary parts of zonal harmonics with zonal wave numbers 1–3 in the meridional wind at the stratospheric middle latitudes to investigate the travelling PWs and tides activity during the time interval considered. The method of separation PWs into the standing and westward/eastward propagating components has been described in Pogoreltsev et al. (2007). Fig. 9 shows the amplitude wavelet spectra of

westward propagating PWs in the meridional wind at latitude 52.5N in the upper stratosphere. The results obtained demonstrate that during time interval of SSW event (end of December 2012 – first half of January 2013) the migrating tides are suppressed. It should be noted that additionally during the main phase of SSW a set of high-frequency PWs (periods 1.5–2 days) with zonal wave numbers 1–3 is generated. All these waves are capable of propagating into the MLT region and can explain the observed differences in behavior of the OH emission intensity, temperature and atomic oxygen concentration over Tory and Zvenigorod.

6. Conclusions

Based on the ground-based spectrometric measurement data on the OH(6-2) hydroxyl emission at the longitudinally spaced Tory (51.8°N, 103.1°E) and Zvenigorod (55.7°N, 36.8°E) stations, by involving the SABER satellite measurement data and the MUAM simulation, the temperature regime and the atomic oxygen concentration in the mesopause region during the 2013 January major sudden stratospheric warming have been analyzed.

As a result of that analysis, we revealed significant variations in the OH emission intensity and temperature, as well as in the atomic oxygen concentration at the hydroxyl emission layer. The observed variations may be explained by an adiabatic expansion or compression of the emission layer due to changes of its height.

Significant longitudinal differences in the behavior of the investigated characteristics have been found. Thus, in the Tory Station region, the OH maximal intensities and temperature, as well as the atomic oxygen maximal concentration, caused by the emission layer height lowering, were observed during the SSW evolution. Over the Zvenigorod Station, the maximal values for those characteristics were observed at the SSW recovery phase.

As a result of numerical modeling, a possible cause for the revealed effect was shown to be longitudinal differences in diurnal variation of the vertical wind at the mesopause heights over the indicated sites during the SSW event. One may elucidate these differences through generation of non-migrating tides due to a non-linear interaction between the intensified stationary planetary wave 1 (SPW1) and migrating tides and forcing a set of high-frequency PWs at the stratospheric heights. All these waves are capably of propagating into the MLT region and produce observed changes in behavior of the OH emission intensity, temperature and atomic oxygen concentration over Tory and Zvenigorod.

Acknowledgments

This study was supported by the Russian Foundation for Basic Research, Grant No. 17-05-00192-a. Numerical simulations with the MUAM were supported by the Russian Foundation for Basic Research under research grant No. 18-05-01050. The experimental data recorded by the Angara Multiaccess Center facilities at the ISTP SB RAS (Tory Station) obtained within the Program of Fundamental Research of State Academies of Russia for 2013-2020, (Project II.16.1.2) were used. We thank the SABER/TIMED team for the access to the temperature and emission rates data, and the MERRA and ERA5 teams for the access to the reanalysis data.

References

Baker, D.J., Stair, A.T., 1988. Rocket measurements of the altitude distribution of the hydroxyl airglow. Phys. Scripta 37 (4), 611–622.

Bates, D.R., Nicolet, M., 1950. The photochemistry of atmospheric water vapour. J. Geophys. Res. 55, 301–327.

Feng, W., Kaifler, B., Marsh, D.R., Höffner, J., Hoppe, U.-P., Williams, B.P., Plane, J.M.C., 2017. Impacts of a sudden stratospheric warming on the mesospheric metal layers. J. Atmos. Sol. Terr. Phys. 162, 162–171.

Gavrilov, N.M., Koval, A.V., 2013. Parameterization of mesoscale stationary orographic wave forcing for use in numerical models of atmospheric dynamics. Izvestiya Atmos. Ocean. Phys. 49 (3), 244–251. https://doi.org/10.1134/S0001433813030067.

Gelaro, R., McCarty, W., Suárez, M.J., Todling, R., Molod, A., Takacs, L., Randles, C.A., Darmenov, A., Bosilovich, M.G., Reichle, R., Wargan, K., Coy, L., Cullather, R., Draper, C., Akella, S., Buchard, V., Conaty, A., da Silva, A.M., Gu, W., Kim, G.-K., Koster, R., Lucchesi, R., Merkova, D., Nielsen, J.E., Partyka, G., Pawson, S., Putman, W., Rienecker, M., Schubert, S.D., Sienkiewicz, M., Zhao, B., 2017. The Modern-Era retrospective analysis for research and Applications, version 2 (MERRA-2). J. Clim. 30 (14), 5419–5454. https://doi.org/10.1175/JCLI-D-16-0758.1.

Hersbach, H., Dee, D., 2016. ERA5 reanalysis is in production, ECMWF Newsletter No. 147. Spring 7.

Hong, S.-S., Wang, P.-H., 1980. On the thermal excitation of atmospheric tides. Bull. Geophys. 19, 56–84.

Kaufman, F., 1969. Neutral reactions involving H and other minor constituents. Can. J. Chem. 47 (10), 1917–1926.

Khomich, V.Yu, Semenov, A.I., Shefov, N.N., 2008. Airglow as an Indicator of Upper Atmospheric Structure and Dynamics. Springer-Verlag, Berlin Heidelberg.

Klimenko, M.V., Klimenko, V.V., Bessarab, F.S., Korenkov, Y.N., Liu, H., Goncharenko, L.P., Tolstikov, M.V., 2015. Study of the thermospheric and ionospheric response to the 2009 sudden stratospheric warming using TIME-GCM and GSM TIP models: first results. J. Geophys. Res. Space Phys. 120, 7873–7888. https://doi.org/10.1002/2014JA020861.

Kobayashi, S., Ota, Y., Harada, Y., Ebita, A., Moriya, M., Onoda, H., Onogi, K., Kamahori, H., Kobayashi, C., Endo, H., Miyaoka, K., Takahashi, K., 2015. The JRA-55 reanalysis: general specifications and basic characteristics. J. Meteor. Soc. Japan 93, 5–48. https://doi.org/10.2151/2015-001.

Krassovsky, V.I., 1963. Chemistry of the upper atmosphere. In: In: Priester, W. (Ed.), Space Research, vol. 3. North-Holland Publ Co, Amsterdam, pp. 96–116.

Langhoff, S.R., Werner, H.J., Rosmus, P., 1986. Theoretical transition probabilities for the OH Meinel system. J. Mol. Spectrosc. 118 (4), 507–529.

Lin, C.L., Leu, V.T., 1982. Temperature and thirdbody dependence of the constant for the reaction O + O2 + M → O3 + M. Int. J. Chem. Kinet. 14, 417.

Medvedeva, I., Ratovsky, K., 2017. Effects of the 2016 February minor sudden stratospheric warming on the MLT and ionosphere over Eastern Siberia. J. Atmos. Sol. Terr. Phys. https://doi.org/10.1016/j.jastp.2017.09.007.

Medvedeva, I.V., Semenov, A.I., Perminov, V.I., Beletsky, A.B., Tatarnikov, A.V., 2014. Comparison of ground-based OH temperature data measured at irkutsk (52°N, 103°E) and Zvenigorod (56°N, 37°E) stations with aura MLS v3.3. Acta Geophys. 62 (2), 340–349. https://doi.org/10.2478/s11600-013-0161-x.

Mitchell, D.M., Gray, L.J., Anstey, J., Baldwin, M.P., Charlton-Perez, A.J., 2013. The influence of stratospheric vortex displacements and splits on surface climate. J. Clim. 26 (8), 2668–2682.

Mulligan, F.J., Dyrland, M.E., Sigernes, F., Deehr, C.S., 2009. Inferring hydroxyl layer peak heights from ground-based measurements from ground-based measurements of OH(6-2) band integrated emission rate at Longyearbyen (78°N,16°E). Ann. Geophys. 27, 4197–4205.

Nicolet, M., 1971. Aeronomic reactions of hydrogen and ozone. In: Fiocco, G. (Ed.), Mesospheric Models and Related Experiments. D.Reidel Publ. Co., Dordrecht, pp. 1–51.

Nicolet, M., 1989. Aeronomic chemistry of ozone. Planet. Space Sci. 37 (12), 1621–1652.

Pancheva, D., Mukhtarov, P., Mitchell, N.J., Andonov, B., Merzlyakov, E., Singer, W., Murayama, Y., Kawamura, S., Xiong, J., Wan, W., Hocking, W., Fritts, D., Riggin, D., Meek, C., Manson, A., 2008. Latitudinal wave coupling of the stratosphere and mesosphere during the major stratospheric warming in 2003/2004. Ann. Geophys. 26, 467–483. https://doi.org/10.5194/angeo-26-467-2008.

Pedatella, N.M., Richmond, A.D., Maute, A., Liu, H.-L., 2016. Impact of semidiurnal tidal variability during SSWs on the mean state of the ionosphere and thermosphere. J. Geophys. Res. Space Phys. 121. https://doi.org/10.1002/2016JA022910.

Perminov, V.I., Semenov, A.I., Medvedeva, I.V., Zheleznov, YuA., 2014. Variability of mesopause temperature from the hydroxyl airglow observations over midlatitudinal sites, Zvenigorod and Tory, Russia. Adv. Space Res. 54, 2511–2517. https://doi.org/10.1016/j.asr.2014.01.027.

Pogoreltsev, A.I., Savenkova, E.N., Pertsev, N.N., 2014. Sudden stratospheric warmings: the role of normal atmospheric modes. Geomagn. Aeron. 54 (3), 357–372. https://doi.org/10.1134/S0016793214020169.

Pogoreltsev, A.I., Vlasov, A.A., Fröhlich, K., Jacobi, Ch, 2007. Planetary waves in coupling the lower and upper atmosphere. J. Atmos. Sol. Terr. Phys. 69 (17–18), 2083–2101. https://doi.org/10.1016/j.jastp.2007.05.014.

Portnyagin, Y.I., Solov'eva, T.V., Merzlyakov, E.G., Pogorel'tsev, A.I., Savenkova, E.N., 2010. Height-latitude structure of the vertical wind in the upper mesosphere and lower thermosphere (70-110 km). Izvestiya Atmos. Ocean. Phys. 46 (1), 85–94. https://doi.org/10.1134/S0001433810010123.

Portnyagin, Y.I., Merzlyakov, E.G., Solov'eva, T.V., Pogorel'tsev, A.I., Suvorova, E.V., Mukhtarov, P., Pancheva, D., 2011. Height-latitude structure of the vertical component of the migrating semidiurnal tide in the upper mesosphere and lower thermosphere region (80-100 km). Izvestiya Atmos. Ocean. Phys. 47 (1), 108–118. https://doi.org/10.1134/S0001433811010117.

Reed, R.J., Recker, E.E., 1971. Structure and properties of synoptic-scale wave disturbances in the equatorial western Pacific. J. Atmos. Sci. 28, 1117–1133.

Rienecker, M.M., et al., 2011. MERRA: NASA's Modern-Era retrospective analysis for research and applications. J. Clim. 14, 3624–3648. https://doi.org/10.1175/JCLI-D-11-00015.1.

Russell III, J.M., Mlynczak, M.G., Gordley, L.L., Tansock, J., Esplin, R., 1999. An overview of the SABER experiment and preliminary calibration results. Pros. SPIE 3756, 277–288. https://doi.org/10.1117/12.366382.

Semenov, A.I., Shefov, N.N., 1996. An empirical model for the variations in the hydroxyl

emission. Geomagn. Aeron. 36, 468–480.
Semenov, A.I., Bakanas, V.V., Perminov, V.I., Zheleznov, YuA., Khomich, YuV., 2002. The near infrared spectrum of the emission of the nighttime upper atmosphere of the Earth. Geomagn. Aeron. 42 (3), 390–397.
Shefov, N.N., 1961. On determination of the rotational temperature of the OH bands. In: Krassovsky, V.I. (Ed.), Spectral, Electrophotometrical and Radar Researches of Aurorae and Airglow (5). USSR Acad Sci Publ House, pp. 5–9.
Shepherd, M.G., Cho, Y.M., Shepherd, G.G., Ward, W., Drummond, J.R., 2010. Mesospheric temperature and atomic oxygen response during the January 2009 major stratospheric warming. J. Geophys. Res. 115, A07318. https://doi.org/10.1029/2009JA015172.
Shpynev, B., Kurkin, V., Ratovsky, K., Chernigovskaya, M., Belinskaya, A., Grigorieva, S., Stepanov, A., Bychkov, V., Pancheva, D., Mukhtarov, P., 2015. High-midlatitude ionosphere response to major stratospheric warming. Earth Planets Space 67, 18. https://doi.org/10.1186/s40623-015-0187-1.
Torrence, Ch, Compo, G.P., 1998. A practical guide to wavelet analysis. Bull. Am. Meteorol. Soc. 79, 61–78.
Tweedy, O.V., Limpasuvan, V., Orsolini, Y.J., Smith, A.K., Garcia, R.R., Kinnison, D., Randall, C.E., Kvissel, O.-K., Stordal, F., Harvey, L., Chandran, A., 2013. Nighttime secondary ozone layer during major stratospheric sudden warmings in specified-dynamics WACCM. J. Geophys. Res. Atmos. 118, 1–13. https://doi.org/10.1002/jgrd.50651.
Wu, Q., Nozawa, S., 2015. Mesospheric and thermospheric observations of the January 2010 stratospheric warming event. J. Atmos. Sol. Terr. Phys. 123, 22–38.
Yee, J.H., Crowley, G., Roble, R.G., Skinner, W.R., Burrage, M.D., Hays, P.B., 1997. Global simulations and observations of O(1S), O2(b1S) and OH mesospheric nightglow emissions. J. Geophys. Res. 102, 968 19,949–19.
Yiğit, E., Medvedev, A.S., 2015. Internal wave coupling processes in Earth's atmosphere. Adv. Space Res. 55, 983–1003.